Geophys. J. Int. (2003) **153,** 289–304

Partial melt or aqueous fluid in the mid-crust of Southern Tibet? Constraints from INDEPTH magnetotelluric data

Shenghui Li,[1] Martyn J. Unsworth,[2] John R. Booker,[1] Wenbo Wei,[3] Handong Tan[3] and Alan G. Jones[4]

[1] *Department of Earth and Space Sciences, University of Washington, Seattle,* WA 98195, *USA. E-mail: shenghui@ess.washington.edu*
[2] *Institute of Geophysical Research, Department of Physics, University of Alberta, Edmonton, Canada*
[3] *Department of Applied Geophysics, China University of Geosciences, Beijing, China*
[4] *Geological Survey of Canada, Ottawa, Canada*

Accepted 2002 August 13. Received 2002 June 21; in original form 2001 July 23

SUMMARY

The INDEPTH project has applied modern geophysical techniques to the study of the crustal structure and tectonic evolution of the Tibetan Plateau. In the Lhasa Block, seismic reflection surveys in 1994 detected a number of bright-spots at 15–20 km depths that indicate zones of crustal fluids (aqueous fluids or partial melt). Coincident magnetotelluric (MT) data collected in 1995 detected a major zone of high electrical conductivity at the same depth as the bright-spots. Using constrained inversion, the MT data require a minimum crustal conductance of 6000 S. This abnormally high electrical conductance can be best explained by a layered model with fluids: partial melt, aqueous fluids or a combination of partial melt and aqueous fluids. The non-uniqueness of the MT method means that a wide range of melt fraction–thickness combinations for the above models could all explain the 6000 S conductance. To distinguish between these three models, other geophysical and geological data are required. Reflection seismic data suggest that a high fluid content (>15 per cent) is present at the top of the layer. The amplitude-versus-offset data suggest that the top of this layer may be aqueous fluids rather than partial melt. Passive seismic data imaged a 20 km thick layer of lower fluid content that is probably partial melt. Petrological studies suggest that concentrations of aqueous fluids above 0.1 per cent at mid-crustal depth cannot be sustained. Taken together, these data show that the high conductivity in Southern Tibet is most probably the result of a relatively thin layer of aqueous fluids (100–200 m) overlying a thicker zone of partial melt (>10 km).

Key words: electrical conductance, electrical conductivity, magnetotellurics (MT), partial melt, saline fluid, seismic bright-spots, Tibetan Plateau.

1 INTRODUCTION

The India–Asia continent–continent collision has created the most spectacular topographic feature on the surface of the Earth. The Tibetan Plateau has an area approximately half the size of the conterminous United States with an elevation above 5 km. It represents a key location for understanding the processes of mountain building and plateau formation during continent–continent collisions. Although our understanding of the geological structure and history of the Tibetan Plateau has significantly improved over the previous two decades, many first-order structural questions are still under debate. Numerous models have been proposed to explain the tectonic processes that have thickened the crust; and span the spectrum from underthrusting of the Indian plate (Argand 1924) to distributed thickening of the Tibetan crust (Dewey & Burke 1973). Other processes that need to be considered include fluid injection into the Tibetan lower crust (Zhao & Morgan 1987), eastward extrusion of the crust and mantle (Tapponnier *et al.* 1982) and southward subduction of Asian lithospheric mantle (Willett & Beaumont 1994).

The first detailed geophysical studies in Southern Tibet were made during Sino–French studies in the 1980s that gave evidence for partial melting from high heat flow and high electrical conductivity (Francheteau *et al.* 1984; van Ngoc *et al.* 1986). The INDEPTH (International Deep Profiling of Tibet and the Himalayas) project was initiated in 1992 to continue the investigation of the structure and evolution of the Tibetan Plateau. The INDEPTH corridor in Southern Tibet extends from the High Himalaya to the centre of the Lhasa Block (Fig. 1). Along this profile active and passive seismic, magnetotelluric (MT) and geological data were collected. Combined with data collected by the Sino–French team, the INDEPTH data suggested that the middle crust beneath Southern Tibet is partially molten (Nelson *et al.* 1996). The evidence for partial melt included high heat flow (Francheteau *et al.* 1984), seismic bright-spots at a depth of 15–20 km (Brown *et al.* 1996), high electrical conductivity

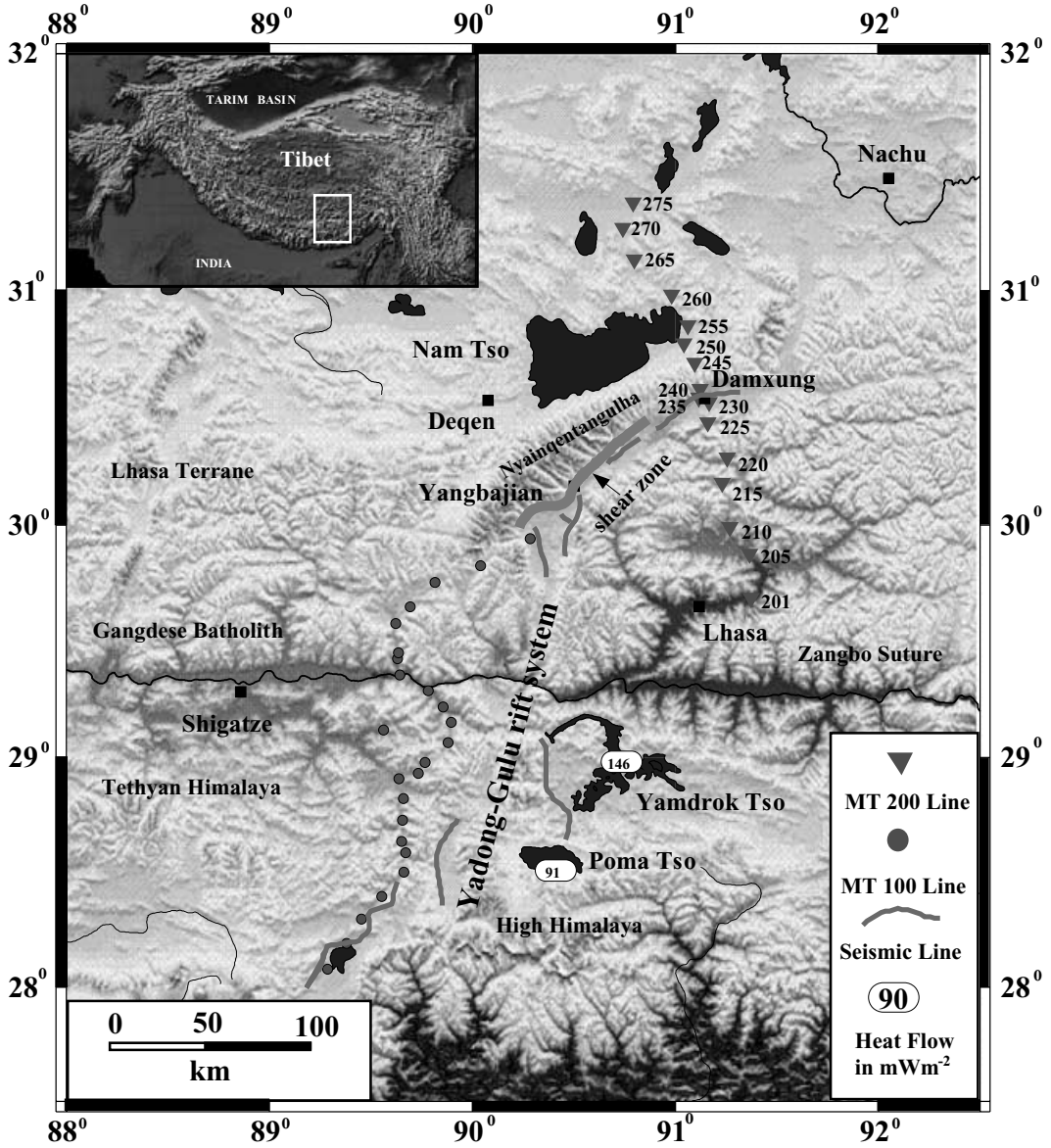

Figure 1. Location map of the INDEPTH MT survey in Southern Tibet. The location of INDEPTH seismic profiles and heat flow measurements made by Francheteau *et al.* (1984) are also shown. This figure is in colour on Blackwell *Synergy*, in the online version of the journal.

(Chen *et al.* 1996; van Ngoc *et al.* 1986), strong *P*-to-*S* wave conversion shown by seismic wide-angle seismic data, and low crustal velocity (Kind *et al.* 1996). Other seismic data give differing views of the composition and degree of melting in the Tibetan crust. A passive seismic study in Tibet (Owens & Zandt 1997) found a low to normal crustal Poisson ratio in the southern plateau, which is inconsistent with a thick, extensively melted middle crust. In addition, Makovsky & Klemperer (1999) showed that a detailed analysis of the wide-angle reflection data could be taken to indicate that the bright-spots may be caused by a thin layer of aqueous fluid.

The presence of partial melt in the crust has important implications for the rheology of the Tibetan crust. A thermally weakened and partially molten crust can behave as a fluid and explain both the flatness of the Tibetan Plateau (Fielding *et al.* 1994) and give evidence for geodynamic models requiring lower crustal flow (Zhao & Morgan 1987; Clark & Royden 2000). If one can conclude that there is no partially molten or fluid layer beneath Southern Tibet, then these geodynamic models of the crust need to be reconsidered. In this study, we will show how MT data can quantify the amount of fluid that is needed to cause the high conductivity in Southern Tibet. Using a constrained inversion, the minimum electrical conductance in Southern Tibet is estimated. This minimum conductance is then used to develop thickness constraints for the mid-crustal high-conductivity zone. Combining the thickness constraints with other geophysical data, we examine the various models that have been proposed for the mid-crustal zone in Southern Tibet and determine whether they are consistent with the MT data. We first give some background information concerning the study region and then present a detailed analysis of the MT data. In conclusion, we suggest that the middle crust conductive zone in Southern Tibet is unlikely to be explained by either partial melts or aqueous fluid alone. The bright-spots in Southern Tibet are most likely a concentration of aqueous fluid overlying a thick, widely distributed layer of partial melt.

2 PREVIOUS STUDIES AND REGIONAL GEOLOGY

The 200-line traverses the Southern Lhasa Block, which is one of the three major terranes accreted to Asian prior to the India–Asia collision (Sengor 1981). The regional geology in the Southern Lhasa Block is characterized by an ancient continental margin. The Palaeozoic and Mesozoic sequence are intruded by the Cretaceous to Tertiary Gandese batholiths that were formed by the northward subduction of the Tethyan oceanic lithosphere prior to the arrival of the India subcontinent (Allegre *et al.* 1984). South of the Nyainqentanghla range, the well-exposed Palaeogene age volcanic rocks may be coeval with the Gandese batholiths (Copeland *et al.* 1995).

The northeast–southwest-trending Nyainqentanghla range and adjacent Yangbajian–Damxung graben were formed by the east–west extension that has formed a number of rift zones in Southern Tibet (Armijo *et al.* 1986). The Nyainqentanghla range represents the footwall of a ductile shear zone that has exhumed mid-crustal rocks (Coward *et al.* 1988; Pan & Kidd 1992). These rocks are dominantly granitic orthogneiss and thermochronology shows that they have been uplifted by approximately 17 km over the last 8 Myr (Harrison *et al.* 1995). Seismic reflection data collected in the Yangbajain–Damxung graben suggest that the Palaeozoic strata in the graben is no thicker than 10 km and is underlain by crystalline basement (Cogan *et al.* 1998). The lack of deep cutting valleys suggests the opening of the rift has been accommodated by lateral mid to lower crustal flow. Within the graben a number of geothermal phenomena have been identified, including the geothermal power plant at Yangbajian (Hochstein & Regenauer-Lieb 1998). The INDEPTH seismic reflection profiles in the graben showed high-amplitude bright-spots, the high amplitude and negative polarity of which strongly suggest the presence of a fluid phase within the middle crust (Brown *et al.* 1996; Makovsky *et al.* 1996). MT data collected on a profile that crossed the graben (200-line, Fig. 1) showed a conductive mid-crustal zone that extended outside the graben (Chen *et al.* 1996). Although the nature of the conductive zone is unclear, the unusually high conductivity on a large spatial scale indicates that a well-connected regional electrical current path must exist. The nature of the fluid that is causing the reflections is unknown, but partial melt and aqueous fluids are the most likely candidates. The presence of each fluid has different implications for the thermal state of the crust, and for the related processes that thickened the crust (Nelson *et al.* 1996; Makovsky & Klemperer 1999). If the observed bright-spots are magma bodies, then partial melt and a high-temperature (>650 °C) middle crust are expected. This hot middle to lower crust may then be weak enough to behave as a fluid layer, as in geodynamic models such as the continental injection model (Zhao & Morgan 1987) or in flow models (Royden *et al.* 1997). On the other hand, an aqueous source for the bright-spots would constrain the thermal state of the crust at the depth of the bright-spots to be lower than 650 °C. Although the existence of aqueous fluid does not exclude the existence of partial melt, the seismic bright-spots and high electrical conductivity can be equally explained by aqueous fluid alone. MT is inherently sensitive to the presence of interconnected fluids. However, determining which fluid is causing the high conductivity requires additional geophysical and petrological data.

3 THE 200-LINE MAGNETOTELLURIC DATA

MT data were collected on two profiles in Southern Tibet in 1995 (Chen *et al.* 1996). The 100-line extended from the High Himalaya to Yangbajian, and the 200-line extended from east of Lhasa, across the Yangbajian–Damxung graben and terminated 50 km north of Nam Tso (Fig. 1). The location of the 200-line was chosen to determine whether there are differences in crustal electrical conductivity within and outside the Yadong–Gulu rift. Long-period MT data were collected using Long-Period MT System (LiMS) designed by the Geological Survey of Canada (20–20 000 s) and broad-band MT data were collected using a single Phoenix V5 system (320–0.001 Hz). The eight long-period MT sites were located roughly 20 km apart. Broad-band MT data were collected at 16 locations. This included all long-period sites, and eight intermediate sites to provide a more detailed image of shallow electrical structure. The long-period data were remotely referenced, but the broad-band data were not and thus may be subject to bias (Gamble *et al.* 1979). The two southernmost sites were excluded from the data set owing to their poor data quality. Data above 1 Hz was excluded from the analysis to avoid problems of bias in non-referenced data.

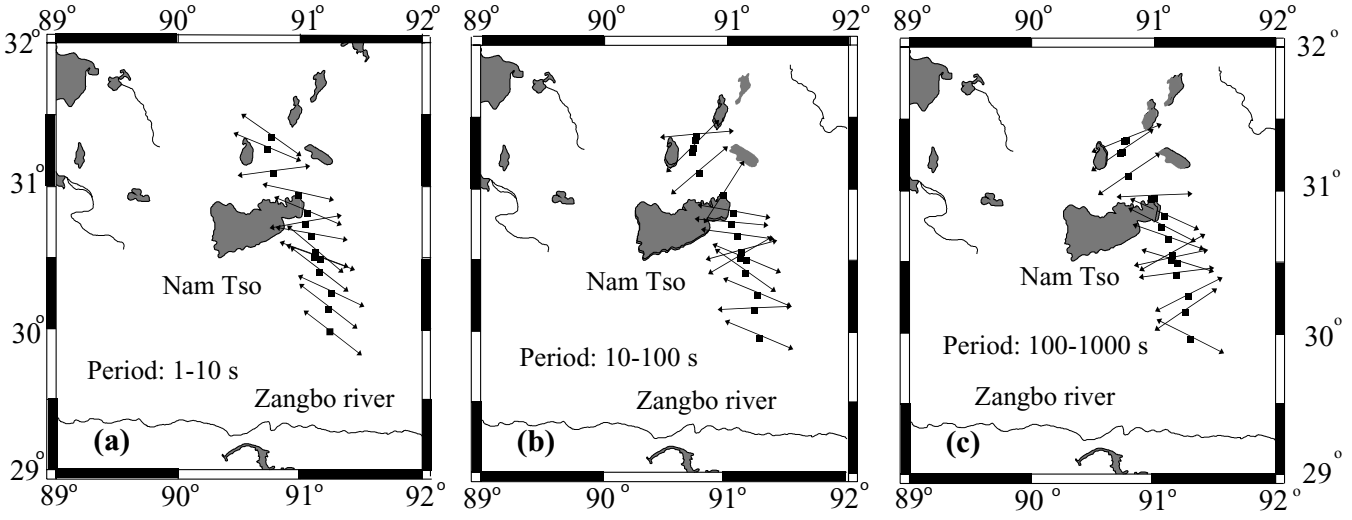

Figure 2. Geoelectric strike for the INDEPTH 200-line. (a) Strike directions for period from 1 to 10 s. (b) Strike directions for period from 10 to 100 s. (c) Strike directions for period from 100 to 1000 s.

The geoelectric strike direction was then calculated using the tensor decomposition technique of Smith (1995) for the three frequency bands shown in Fig. 2. Note that strike directions derived from tensor decomposition have an inherent ambiguity of 90°. At short periods (1–10 s), the strike is roughly W30°N (or N30°E). The strike direction rotates counter-clockwise as the period increases. In the longest-period band, an east–west strike is indicated by the data. Note that a north–south strike is also consistent with the MT data in this period band. This 90° ambiguity can be resolved by using external information, such as the trend of regional geology. In this case, an east–west strike following the sutures and terranes is clearly far more reasonable than a north–south strike. The period dependence of the geoelectric strike shows that the MT data for the 200-line are not purely 2-D with a single-strike direction. There are clearly some 3-D effects present that may be a result of the fact that the graben is not parallel to the regional east–west terrane boundaries. To investigate the effect of strike on the inversions, we consider two possible geoelectric strikes throughout the following analysis; one east–west (Zangbo strike, N90°E) and the other northeast–southwest, reflecting the trend of the graben (graben strike, N45°E). In a 2-D situation, MT data can be separated into two independent modes. The transverse magnetic (TM) mode has electrical currents flowing across the strike while electrical currents flow along the strike in the transverse electric (TE) mode. In the inversion models, we look for conductivity features that are independent of the choice of strike direction. The observed MT data in Zangbo coordinates are shown in pseudosection form in Fig. 3(a). The short-period data ($T < 10$ s) exhibit relatively high values of apparent resistivity and low phases, which implies that the shallow structure is resistive. At longer periods ($T > 10$ s), the phases increase and the apparent resistivities decrease, indicating an increase in conductivity with depth across the whole profile. Two typical sites are shown in Fig. 4. Site 220 is south of Damxung while site 240 is located within the graben. The differences between TE and TM modes indicate that these data are multidimensional, since a 1-D earth produces MT responses that are identical at all azimuths.

4 CONSTRAINED INVERSION OF THE 200-LINE DATA

The inversion of MT data yields a subsurface conductivity model that may be non-unique in a number of aspects. Before discussing the 2-D inversion of the data, it is important to understand the essential physics of the MT method. The depth to the top of a conductive layer and the conductance of the layer are well constrained by the MT data. This is illustrated with a synthetic example. Fig. 5(a) shows the effect of varying the depth of a conductive layer. The MT responses from these models are essentially the same at periods of less than 0.2 s, but large differences can be seen in the responses at periods greater than 0.5 s. The MT responses of these models differ significantly (10° in phase) and show that a 5 km difference in depth could easily be resolved.

To determine the sensitivity of the 200-line MT data to the depth of the conductor, a model study was performed on the model with Zangbo strike and the basement at 100 km (Fig. 7). We fixed the upper 10 km of the model and moved the lower part of the model up and down. The overall rms misfit of the new models is shown in Fig. 6(a). The misfit plot shows a clear minimum at 0 km and indicates that our model is the best-fitting model and that a change of the conductor depth will result in a worse fit. The phase responses of different models and the measured data at site 220 are shown in Fig. 6(b). The difference between the data and model response could not be resolved when the model is shifted 1 km. A shift of 3 km produces a difference comparable to the data errors and could be discerned. A 5 km change would be readily detected. Based on both synthetic and real MT data modelling, we are

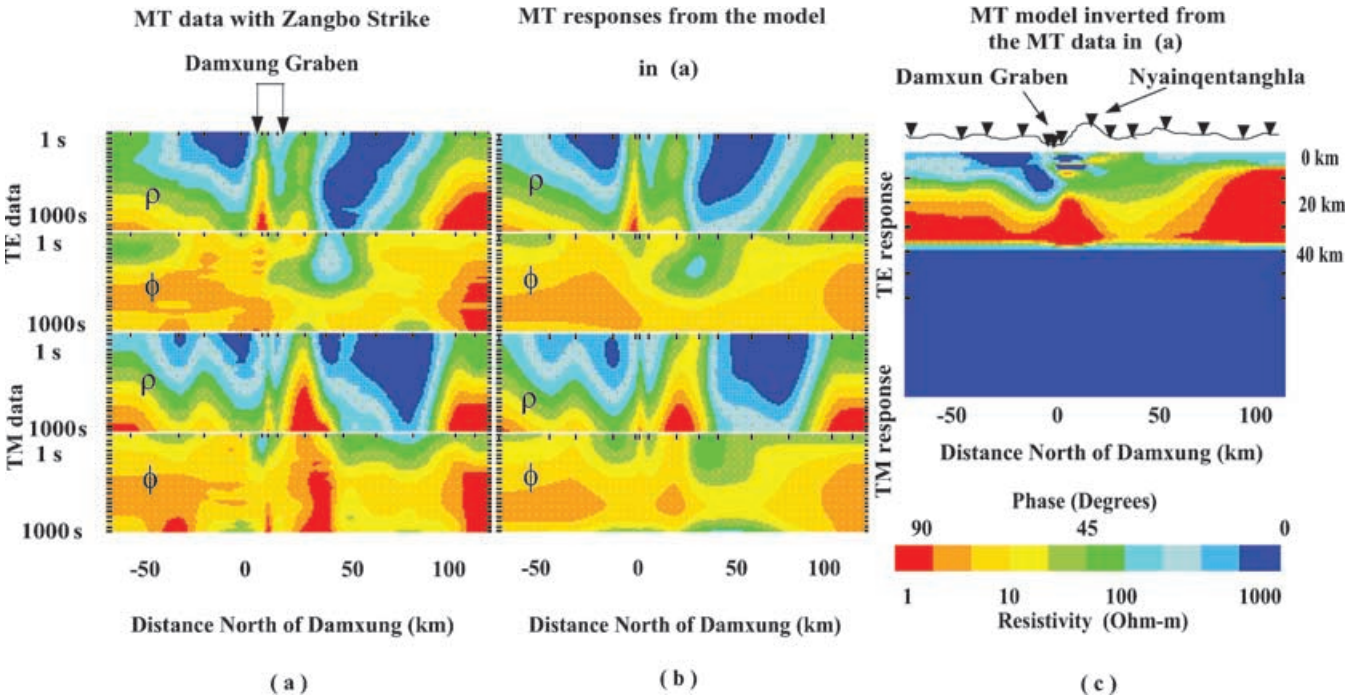

Figure 3. (a) 200-line pseudosections of MT data in measurement coordinates. Periods are shown on a $\log_{10}$ scale. (b) Pseudosections of the MT responses of the inversion model in (c). (c) Inversion model using east–west strike direction with a 1000 Ω m basement fixed at 40 km depth. The site locations and local topography are also sketched on top of the model.

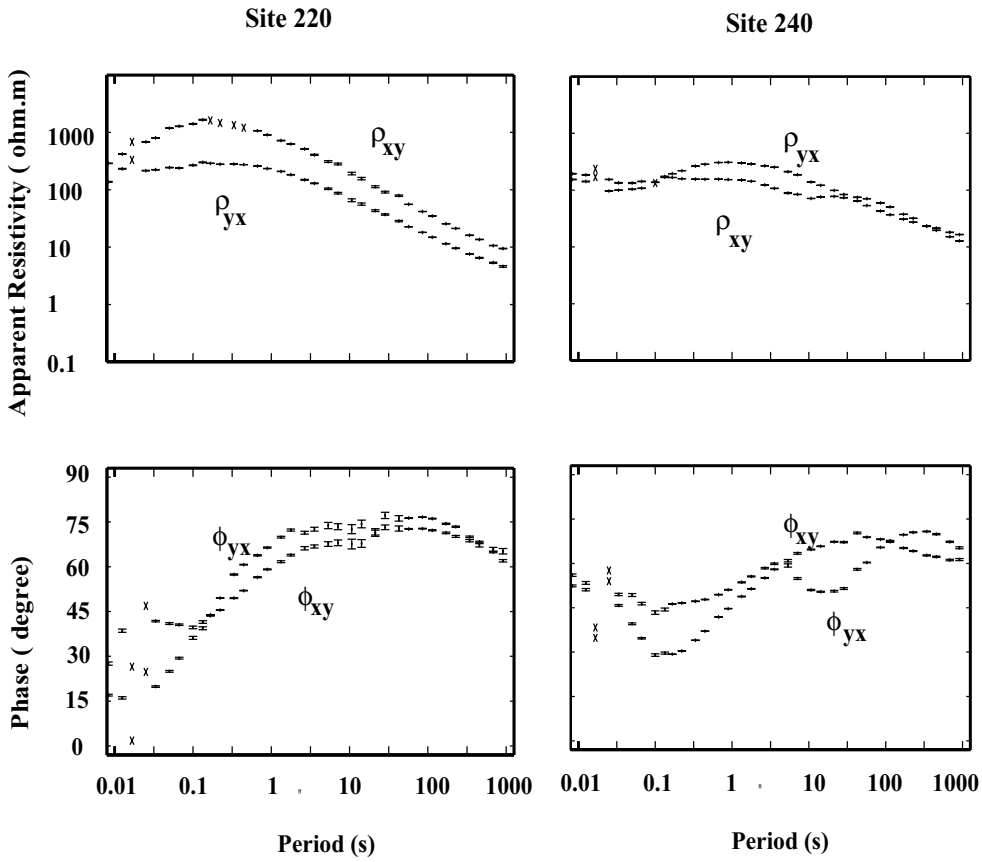

Figure 4. Measured MT data at site 220 (south of the graben) and 240 (within graben.). Data are shown in the measurement coordinate (*x*, NS and *y*, EW). An 'x' indicates that this datum has been excluded owing to poor quality. Note that error bars are relatively large around 10 s in the so-called dead band owing to a low signal-to-noise ratio.

confident that the depth of the conductor is constrained to within 3 km.

Fig. 5(b) shows the important result that the thickness of a layer cannot be constrained by MT data. In each model the conductance of the middle layer is 8000 S, but the thickness and conductivity vary. In the period range 0.01–10 s the apparent resistivity responses of these models are identical. At periods greater than 10 s, only small differences in apparent resistivity and phase can be discerned between the three models. The maximum difference in phase and resistivity is less than 2.5° and 4 Ω m, respectively. These values are comparable to typical errors in field data, and thus to first order, the MT responses of the three models are indistinguishable if the conductance is constant. While the extension of this concept to 2-D and 3-D has not been examined rigorously, the situation is broadly similar if the conductive layer is nearly horizontal. Given a set of MT data, inversions may find different models that can fit the data, but a constant conductance should be expected.

In the context of constraining the nature of the proposed crustal fluid, the minimum conductance required by the data is an important quantity to be determined. If the minimum conductance and the maximum conductivity of a layer can be derived, then the minimum thickness of a conductive layer can be estimated. The minimum conductance is the lower bound on the model conductance that is required by a given set of data. For MT data of limited bandwidth, it may not be possible to sense the bottom of a conductor. This leads to a problem if the inverse algorithm uses a maximum smoothness constraint to make the model unique. The algorithm will simply smear the conductor to infinite depth and give a conductance that is too large. To solve this problem, we replace the model below a given depth with a resistive half-space. If the MT data cannot sense the bottom of the conductive layer, then the resistive region will not affect the data misfit. By moving the top of the resistive half-space upwards until the data can no longer be fitted, we find the shallowest conductor bottom permitted by the data and hence the minimum conductance. This process is referred to as constrained inversion.

In the following inversions, an error floor of 2.86° has been used for all phase data (which is equivalent to a 10 per cent error in apparent resistivity) and 20 per cent for apparent resistivity data. Data errors smaller than this floor level are replaced with the floor value. An error floor is needed for several reasons. First, if the MT data have standard errors that are too small then trying to fit these errors will result in an artificially rough model (Parker 1980). This occurs because uncertainties in the MT data do not just originate in the time-series analysis, but also in geological noise (such as 3-D effects not accounted for in the distortion analysis or 2-D inversions). Finally, MT data usually exhibit frequency bands that have smaller data errors than others. In the absence of an error floor, the inversion will preferentially fit the frequency band with smallest errors, ignoring data in other bands. Hence, with an error floor, a better overall fit to the frequency dependence of the MT data will be obtained. Apparent resistivity data are more susceptible to near-surface distortions than phase data so a lower error floor is used for phase data.

The data were inverted using the rapid relaxation inversion (RRI) algorithm of Smith & Booker (1991). To invert for the minimum

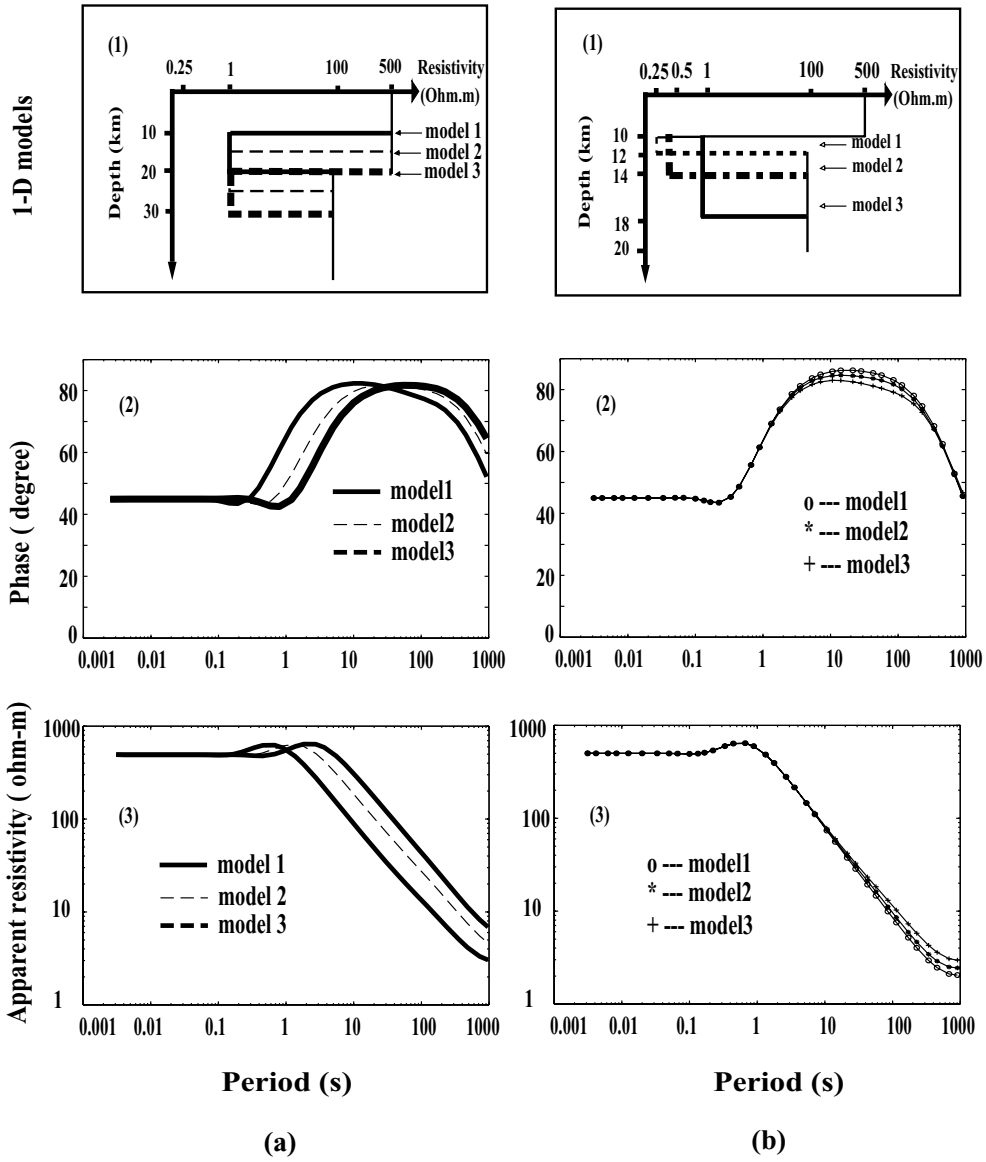

Figure 5. 1-D models and their MT responses. (a1) Three 1-D models with fixed layer thickness and conductivity but the top of the layer varies. (a2) Phase responses of the three models in (a1). (a3) Apparent resistivity responses of the models in (a1). (b1) Three 1-D models with an 8000 S conductor but the layer thickness and conductivity vary. (b2) Phase responses of the three models in (b1). (c) Apparent resistivity responses of the three models in (b1).

conductance required by the data, a low-conductivity (0.001 S m^{-1}) half-space was added to the starting model at a depth of 100 km. The conductivity below this depth was fixed, and thus the inversion algorithm was forced to place all the conductive structure required by the MT data above this depth. This process was then repeated with a progressively shallower resistive basement. In each inversion, both the TE and TM mode data were fitted. The inversions were then repeated with the geoelectric strike in the alternative NE–SW direction. The inversion was started from a 1-D layered model (a conductive layer over the resistive basement) and allowed 15 inversion steps followed by 20 smoothing steps. At this point, the data misfit had converged and the model roughness was decreasing very slowly. The models derived from these inversions for both geoelectric strikes are shown in Fig. 7. In Fig. 3(b), a model and its MT responses are shown. Except for site 250 on the north side of the Nyainqentangula, the model response fits the observed data quite well. Note that the shallow structures are very similar to the model of Chen *et al.* (1996), even though the model is fixed to 0.001 S m^{-1} below 40 km. Fig. 7 also shows the final rms misfit for each model. It can be seen that in order to fit the measured data, the resistive basement needs to be deeper than 20 km. When the resistive basement begins at a depth greater than 20 km, the misfit is independent of basement depth. However, when the basement is at 15 km depth, the misfit increases significantly. This is illustrated in Fig. 8 where the fit to the data is shown at a typical site (TBT220). The data can be adequately fitted when the basement is at 20 km or deeper, but not when it is 15 km. It must be stressed that the depth to the base of the resistor does not have a physical significance. It is the conductance of these models that is to be interpreted. It should be remembered from Fig. 5(b) that, in principle, an infinitely thin layer of finite conductance could also fit the data. The failure of the inversion algorithm to fit the data when the basement is very shallow is just a consequence of the smoothing used in the inversion.

Fig. 9 shows the static shift coefficients computed by RRI for the models in Fig. 6. The static shift coefficients at each site become more positive as the basement becomes shallower. With the

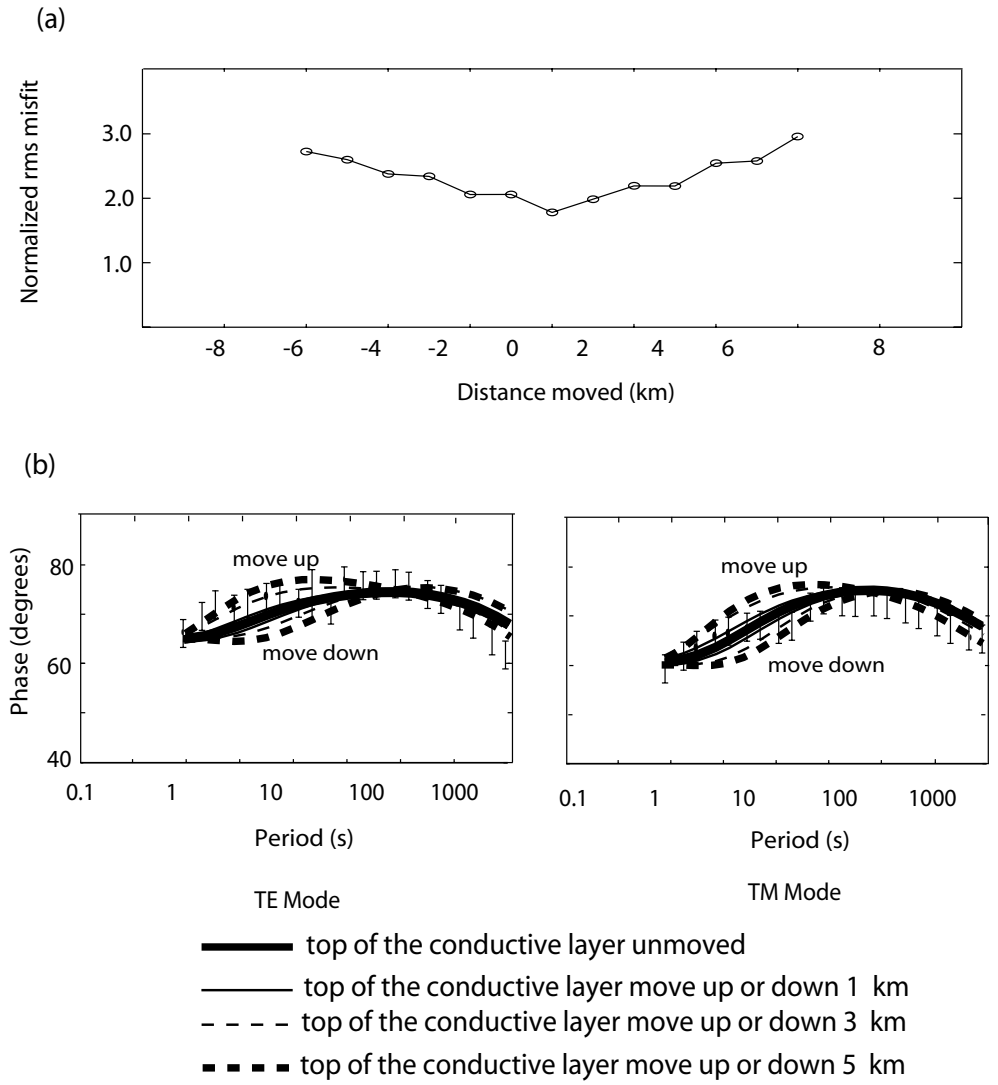

Figure 6. (a) Overall misfit of models with the upper 10 km fixed and the lower part model shifted up and down. (b) MT data and model responses at site 220.

basement deeper than 30 km, the average static shift coefficients are close to zero and the static shift for different basement depths are very close. With the basement at 15 km, the static shift coefficients are significantly more positive than with the basement at 20 km depth. Thus it can be seen that there is a trade-off between the basement depth and the average static shift when the basement is shallower than 30 km. A non-zero average static shift could arise naturally in the data from a structure where the spatial scale is larger than the survey. However, it is more likely that it is produced as an artefact of the inversion as it struggles to fit the data. This is suggested by the fact that the data can be fitted with an average static shift near zero when the basement is deeper than 30 km. The non-uniqueness of the MT model can be clearly seen in Fig. 7. Despite differing strikes and basement depths, each of these models fits the measured data to a reasonable level. Even though these models appear to be quite different, they all exhibit the same resistive upper layer and conductive layer of relatively uniform depth and conductance. Thus the existence of a conductive middle crust is not dependent on the choice of electrical strike. It should also be noted that in all models, the conductive crustal layer extends across the entire profile and is not confined to the graben.

The integrated conductance above the resistive basement for each model is shown in Fig. 10. At Damxung the minimum conductance is 6000 S, but could be as high as 30 000 S. In order to constrain the lower bound on the thickness of a conductive layer, we will only consider the minimum conductance of these models. This crustal conductance is unusually high, since in stable continental regions a lower crustal conductance of 20–2000 S is considered typical (Jones 1992). For comparison, 2 km of seawater has a conductance of 6000 S.

5 ORIGIN OF HIGH CONDUCTIVITY IN SOUTHERN TIBET

Most silicate and carbonate minerals have a low electrical conductivity. Thus to produce a high electrical conductivity, as observed in Tibet, a conducting phase must be present to allow electric current to flow through the rock. Conductive materials that can be found in the Earth include metallic minerals, graphite, molten rock and aqueous (ionic) fluids (Jones 1992). In this section we consider each of these to determine whether they could explain the high conductivity observed in Southern Tibet.

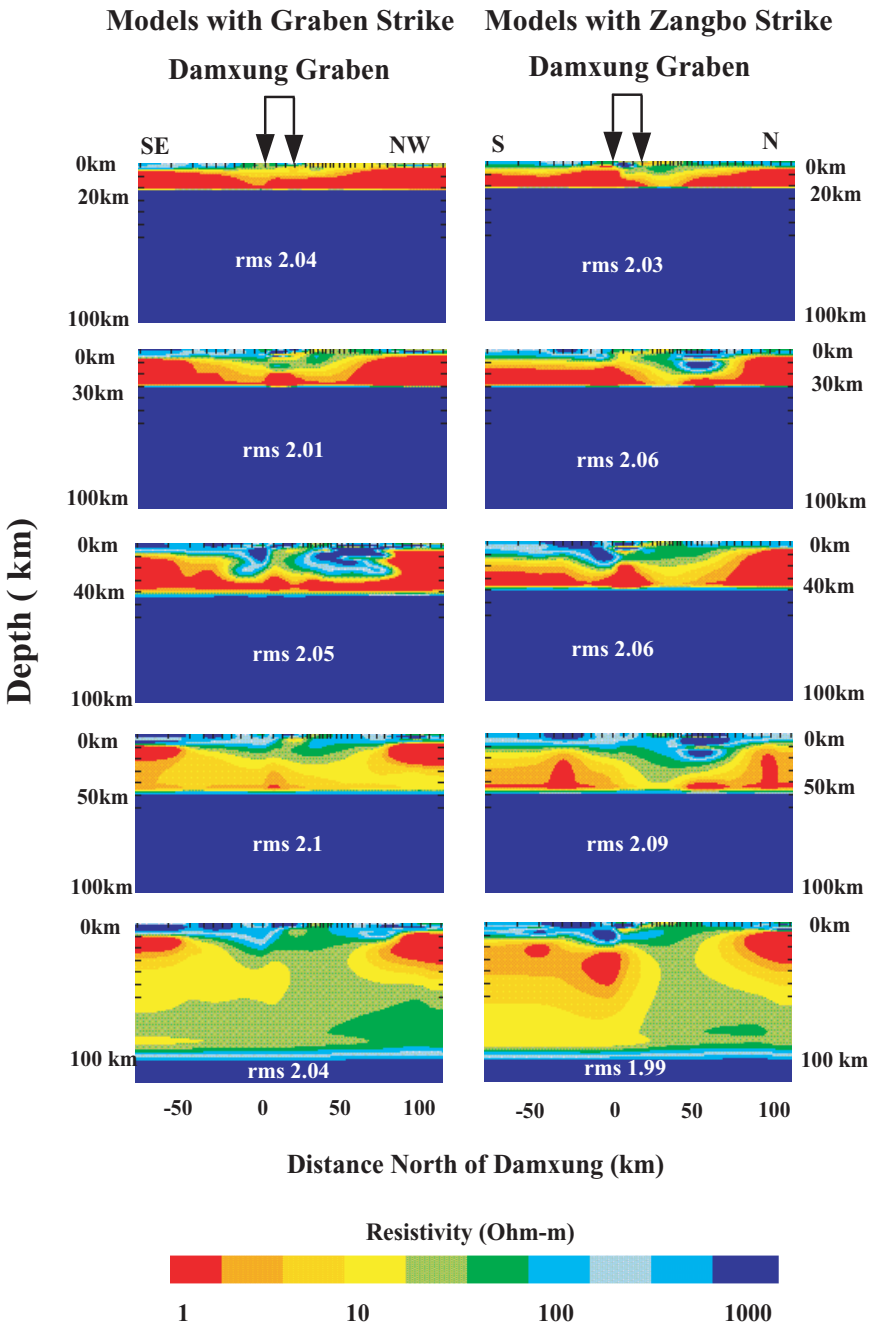

Figure 7. Conductivity models inverted from the 200-line data. Models on the right are inverted using the east–west Zangbo strike and those on the left using the northeast–southwest (graben) strike. Notice the increase in electrical conductivity (red colour) as the basement is moved up.

5.1 Conducting minerals

Metallic ore minerals such as iron and copper sulphides have a very high electrical conductivity (100 S m^{-1}). While they often occur in discrete ore bodies, they can also be disseminated throughout a larger volume. In Southern Tibet, there are several reasons why it is unlikely that these minerals are responsible for the mid-crust conductive layer. First of all, the spatial extent of the conductive layer is very large and it crosses major terrane boundaries. Mineralization is usually associated with specific geological formations and it would be expected to correlate with key geological units. In addition, a large-scale mineral deposit would probably produce detectable gravity and magnetic anomalies that are not observed. Thirdly, mineralization is inconsistent with the INDEPTH seismic data that provided evidence for mid-crustal fluids (Makovsky & Klemperer 1999; Ross *et al.* 2001).

5.2 Grain boundary graphite films

Graphite occurs widely in the Earth and exhibits a very high (but anisotropic) electrical conductivity. When the graphite films on grain boundaries are connected over a significant distance, they can produce a crustal layer with bulk conductivity above 1 S m^{-1} (Frost *et al.* 1989). Nover *et al.* (1998) show that connected

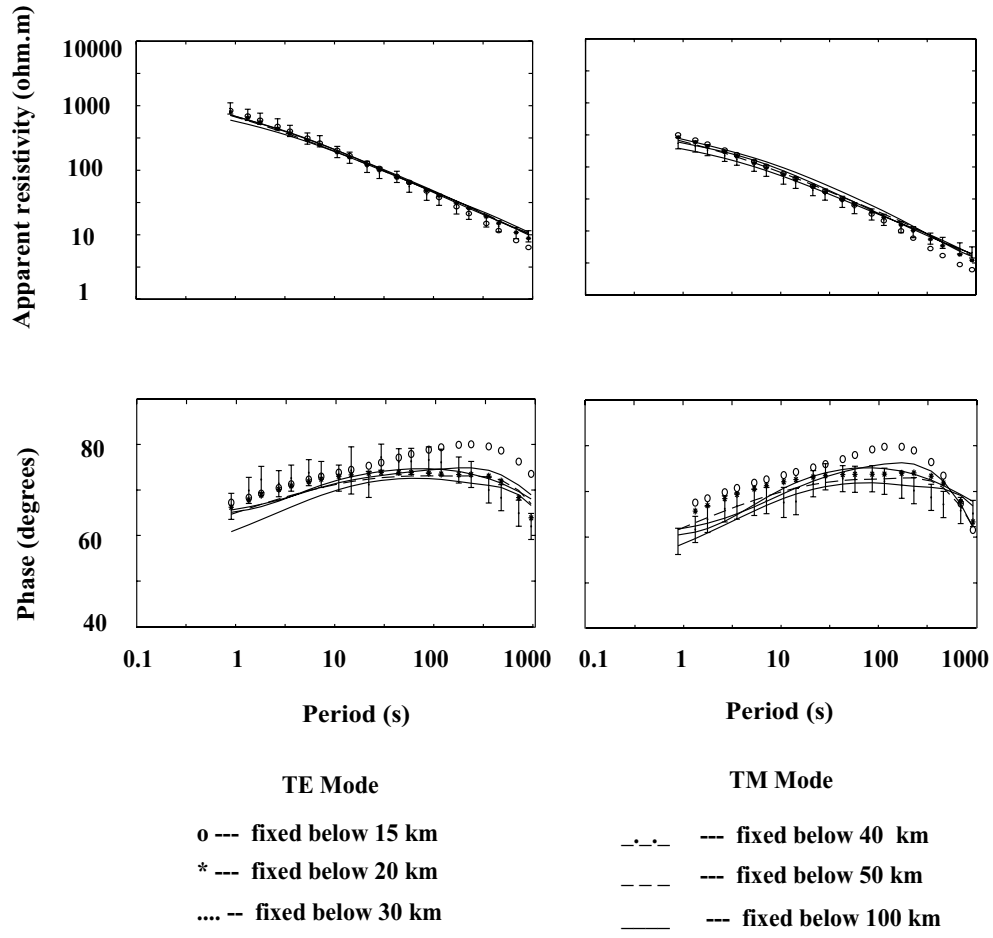

Figure 8. TE and TM responses of a set of models with an east–west (Zangbo) strike and observed data at site 220. Note that when the resistive basement is below 20 km, model responses fit the measured data reasonably well while the response of the model with a 15 km basement deviates from the observed data after 100 s.

networks of carbon and ilmenite are responsible for the enhanced crustal conductivity near the KTB in Germany. The North American Central Plain Anomaly (the largest electrical conductivity anomaly in North America) may be the result of graphite films in a Proterozoic orogen (Camfield & Gough 1977). The stable continental lower crust is unexpectedly conductive and one candidate for the high conductivity is graphite. Thus graphite must be considered as a serious candidate for the cause of high conductivity beneath Southern Tibet. However, there are a number of lines of evidence to suggest that graphite is not responsible for the high conductivity.

(1) For graphite to be an effective conductor the films must remain connected, and while this is often the case in subducted metasediments, it is generally not the case in crystalline basement rocks. In the study area in Southern Tibet, the geological and geophysical data reviewed earlier in this paper confirm that the basement rocks are crystalline (Pan & Kidd 1992; Cogan *et al.* 1998).

(2) An additional piece of evidence for the high conductivity not being caused by graphite is the large spatial extent of the conductive anomaly. It crosses regional geological boundaries and three major terrane boundaries (Wei *et al.* 2001). Given the different geology and tectonic histories of these terranes (Yin & Harrison 2000), it is unlikely that the high conductivity results from a common geological process that produced graphite across the entire plateau.

(3) Graphite could cause high conductivity in the mid-crust in Southern Tibet, but it is hard to reconcile with the seismic data collected in the same region. The high reflectivity and the negative polarity of the reflection (Makovsky & Klemperer 1999; Ross *et al.* 2001) are inconsistent with grain boundary graphite films.

(4) It is possible that graphite exists locally in Southern Tibet in rock units such as granitic orthogneiss that are exposed in the study area. However, even in these rocks, the processes of exhumation and cooling would probably break the connections between films. Thus the rock would not have a high overall conductivity.

Thus in summary, it is unlikely that graphite is the cause of the pervasive high conductivity observed across the Tibetan Plateau.

5.3 Partial melting

5.3.1 Electrical conductivity of pure melts

Owing to the abundance and high mobility of ions, molten rock is a good electrical conductor. The conductivity of pure melt depends on temperature, pressure, the amount of structurally bound and free water and oxygen fugacity (Lebedev & Khitarov 1964; Waff & Weill 1975; Tyburczy & Waff 1983). Dry rocks begin to melt at around 1200 °C and this produces a large increase in conductivity. For dry rocks of various compositions the conductivity of

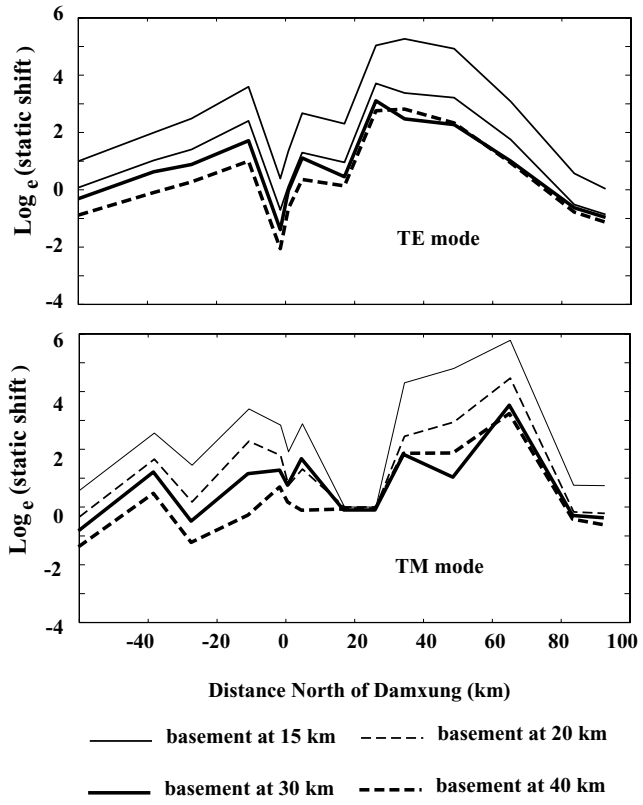

Figure 9. Static shift coefficients for 200-line data with a Zangbo strike.

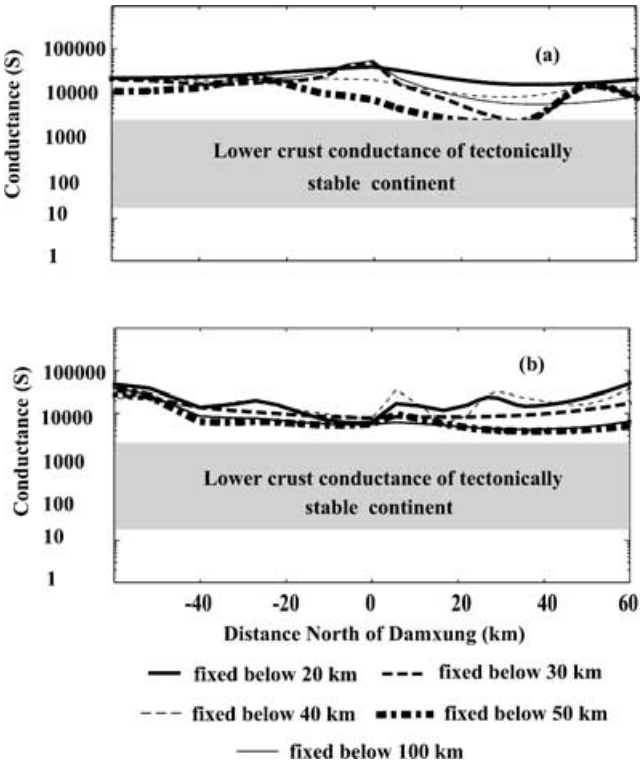

Figure 10. The model conductances for the Tibet MT 200 line. (a) Conductances are shown for five models with the Zangbo strike. (b) Conductances are shown for five models with the graben strike.

pure melt is typically in the range 1–10 S m^{-1} (Tyburczy & Waff 1983). The conductivity increases with temperature and decreases with pressure, but does not exceed 10 S m^{-1} (Tyburczy & Waff 1983). Water-saturated rocks will begin to melt at lower temperatures, typically 650 °C (Lebedev & Khitarov 1964). Again, the melt conductivity increases with temperature and typical conductivities are in the range 1–20 S m^{-1}, slightly higher than for dry melting (Fig. 11).

To estimate the possible melt conductivity in Southern Tibet, the most important parameters are the temperature and water content of melt at a depth of 15–20 km. Heat flow measurements give evidence of high thermal gradients, and Francheteau *et al.* (1984) suggest that the 600 °C isotherm lies at a depth of 10–25 km in Southern Tibet. Alternative evidence for crustal temperatures comes from the thermal history of rocks exhumed in the footwall of the Nyainqentangla Shear Zone. Harrison *et al.* (1995) inferred temperatures of 600–700 °C at a depth of ∼17 km. Geological studies of Himalayan granites suggest that crustal anatexis (melting) occurred in the presence of water (Debon *et al.* 1986; Guillot *et al.* 1995; Scaillet *et al.* 1995). Geodynamic modelling and earthquake studies give indirect information on the temperature at depth (Chen & Molnar 1983; Henry *et al.* 1997) and suggest temperatures at depths of 15–20 km could be as low as ∼400 °C or as high as 700 °C. These lines of evidence suggest that temperatures in the mid-crust are too low for dry melting, but hydrous melting is possible and a range of melt conductivity 1–10 S m^{-1} is to be expected (Fig. 11).

5.3.2 Interconnection of partial melts and bulk resistivity

The electrical conductivity of silicate minerals is much lower than that of pure melt. Thus when a rock is partially molten, the bulk conductivity of the rock depends on the amount of fluid and the interconnectivity of the fluid (Schmeling 1986). The interconnectivity is a key parameter since as soon as a connected fluid network is formed, electric current can flow along the conductive fluid paths and the overall conductivity of the rock will increase dramatically. Several numerical models can be used to calculate the bulk conductivity of the rock for the possible geometric distributions. These include Archie's law (Archie 1942) the Hashin–Shtrikman (HS) upper and lower bounds (Hashin & Shtrikman 1962) and the modified bricklayer model (Macdonald 1987). While these models use different parameters to simulate the bulk conductivity of two-phase mixtures, they are all based on simple parallel and series models (Maxwell 1881). For the HS upper bound the rock matrix and melt are in parallel and the overall conductivity of the circuit is dominated by the most conductive element (melt). For the HS lower bound, the rock matrix and melt are in a series circuit and the overall conductivity is dominated by the resistive rock matrix.

What degree of interconnectivity should we expect for partial melt? Laboratory experiments show that melt can form an interconnected network at melt fractions below 5 per cent (Minarik & Watson 1995; Mibe *et al.* 1998). Roberts & Tyburczy (1999) reported that melt is typically found in tubes along grain boundaries and interconnects at relatively low (<6 per cent) melt fractions. Thus the bulk conductivity was close to the HS upper bound. Fig. 12 shows the relationship between the bulk conductivity of a rock and the fluid (melt) fraction when the fluid (melt) is interconnected. Note that even a small amount of fluid can significantly increase the overall conductivity of the rock. However, as the fluid fraction increases, the bulk conductivity increases rapidly and the curves for different fluid conductivities separate. When the fluid fraction is higher than

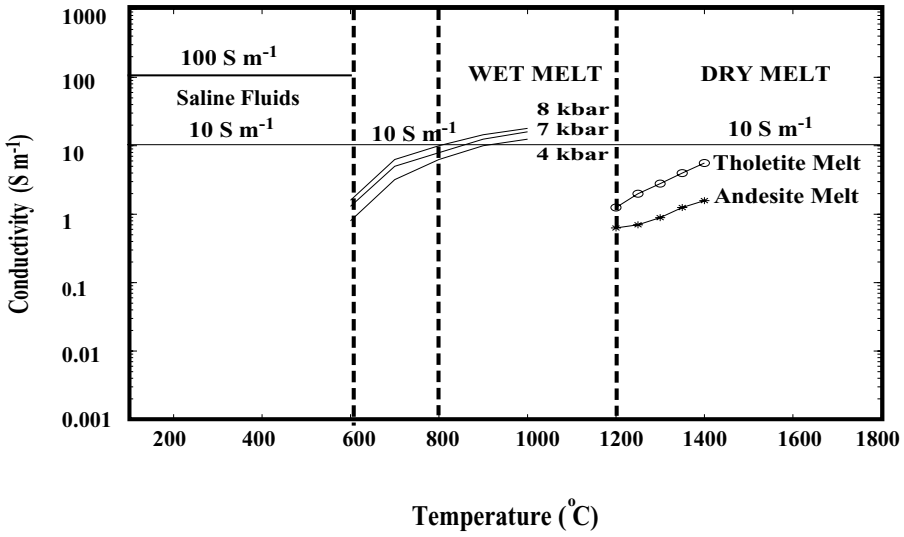

Figure 11. Electrical conductivity of melts and saline fluid. The maximum conductivity for saturated saline fluid is 100 S m^{-1} at temperature lower than 650 °C and the maximum conductivity for melt in Southern Tibet is 10 S m^{-1} with a temperature of 800 °C. Wet melt data are from Lebedev & Khitarov (1964) and dry melt data are from Tyburczy & Waff (1983).

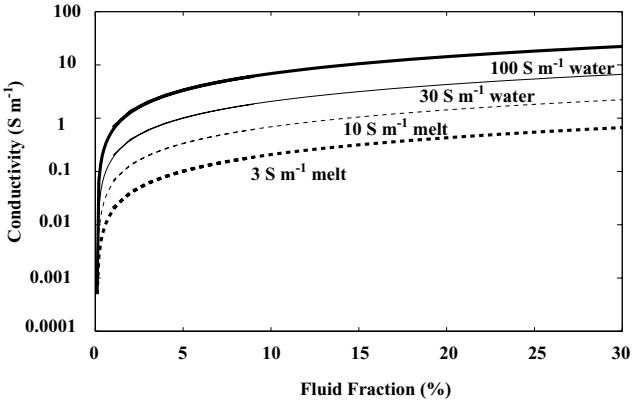

Figure 12. Bulk conductivity of fluid-bearing rocks. Curves are calculated using Hashin–Strikman upper bound and the solid rock conductivity is 0.0005 S m^{-1}. The conductivity of saline fluid used are 100 and 30 S m^{-1} and for melt are 10 and 3 S m^{-1}.

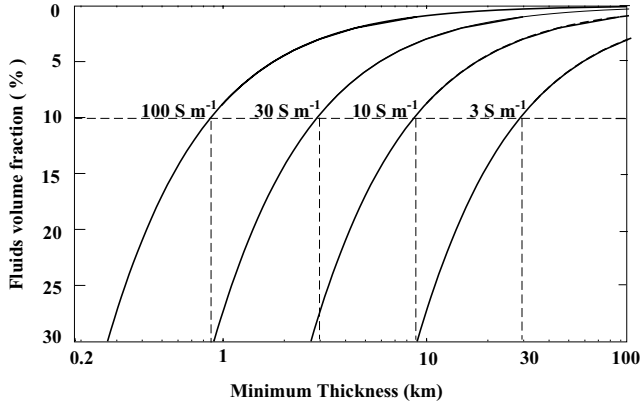

Figure 13. Thickness as a function of fluid fraction and fluid conductivity. Many combinations of thickness, fluid fraction and fluid conductivity can produce the 6000 S conductance required by the MT data. Given a range of fluid conductivities (3–100 S m^{-1}) and 10 per cent fluid fraction, the minimum thickness required by MT data varies from 0.9 to 30 km.

5 per cent, the bulk conductivity is close to a linear function of fluid fraction as conduction through the melt dominates.

5.3.3 Thickness of a melt layer and consistency with other geophysical data

To account for the minimum conductance of 6000 S, a layer of partial melt can have a range of porosity–thickness combinations. This is illustrated in Fig. 13, where it can be seen that as the melt fraction rises, the thickness of the layer decreases. For example, if the layer comprised 10 per cent partial melt, with 10 S m^{-1} melt conductivity, then it would need to be 9 km thick. Note that in the above calculations, it is assumed that the melt conductivity is at the upper limit of the range of possible values. Thus this thickness is a minimum bound for a layer of 10 per cent partial melt. Fig. 13 shows the same information, for a lower melt conductivity of 3 S m^{-1}. With 10 per cent partial melt, a layer ∼30 km thick is required to produce the minimum conductance of 6000 S. Lowering the percentage of partial melt requires a thicker layer. It should be emphasized that because of the physics of the MT method (Fig. 5), MT cannot distinguish between models of equal conductance (i.e. a high melt fraction, thin layer will give the same observed response as a thick, lower melt fraction layer). Thus, other petrological and geophysical observations are needed to discriminate between models having the same conductance.

What melt fraction might be present in Southern Tibet? It has been suggested that the leucograntites of the High Himalaya originated in the partially molten Tibetan crust. A geobarometric analysis of these rocks suggested that the Gangotri leucogranite was derived from a zone with 5–7 per cent melting at 700–800 °C (Scaillet *et al.* 1995). These observations give indirect evidence for relatively high melt fractions. Seismic data give more direct constraints on melt fraction since they were collected in the same place and time as the INDEPTH MT data. These data comprise observations of low-velocity, high reflection coefficients at the top of the low-velocity zone and measurements of Poisson's ratio.

Low-velocity zone (LVZ). Kind *et al.* (1996) reported a low-velocity zone coincident with the 200-line that was approximately 20 km thick. If partial melt is responsible for both the low velocity and low resistivity, then Fig. 12 can be used to compute the melt fraction for a given melt conductivity. With a conductivity of 10 S m^{-1}, a melt fraction of 4 per cent is required. If the melt conductivity is only 3 S m^{-1} then 14 per cent partial melt is needed.

Poisson's ratio. Another parameter that can be used to quantify the amount of fluid in the crust is Poisson's ratio, which varies between 0.25 and 0.5 for continental crust (Zandt & Ammon 1995). Since pure fluid has a Poisson ratio of 0.5, an increase of the bulk Poisson ratio (>0.3) may indicate the existence of fluid in the crust (Owens & Zandt 1997). In Southern Tibet the crust has a low-to-normal average Poisson ratio (Owens & Zandt 1997). While this appears to be inconsistent with the presence of partial melting, Nelson *et al.* (1999) showed that the average value could be achieved with a 20 km thick, 10 per cent mid-crustal partial melt layer, sandwiched between a low Poisson ratio upper crust and a normal Poisson ratio lower crust.

Reflection coefficients. Is a model with a uniform layer of 4–14 per cent partial melt consistent with the reflection coefficients reported for the seismic bright-spots? (Makovsky & Klemperer 1999; Ross *et al.* 2001). The reflection coefficients of −0.4 to −0.6 suggest a fluid fraction in excess of 15 per cent water or melt (Ross *et al.* 2001). Applying the study of Watanabe (1993) to Southern Tibet, the low seismic velocities ($V_p = 3.0 \pm 0.8$ km s^{-1} and $V_s = 1.6 \pm 0.8$ km s^{-1}) and $V_p/V_s \sim 0.5$, suggest a fluid fraction of ∼15 per cent (Makovsky & Klemperer 1999). Thus the reflection data suggest a higher melt fraction than the broad LVZ. These observations can be partially reconciled by a composite model with a layer of pure melt over a zone of partial melt. Magma bodies of this type have been detected in seismic studies of mid-ocean ridges (Navin *et al.* 1998). Seismic waveform modelling of the Southern Tibet data shows that a 37 m thick layer of pure melt over a 185 m partial melt layer (Fig. 14, model 1) could produce the observed waveforms (Ross *et al.* 2001). However, this model has a conductance of just 600 S if the melt has a conductivity of 10 S m^{-1}. With a melt conductivity of 3 S m^{-1}, the layer conductance is only 200 S. Clearly, additional melt at greater depths is needed to produce the minimum 6000 S conductance observed in Southern Tibet. Thus a thin layer with a high melt fraction overlying a zone of 4–14 per cent melting is consistent with the observed conductance, low-velocity and reflection coefficients.

There are other data that are consistent with the occurrence of partial melting in Southern Tibet. This includes geological observations that imply that widespread crustal melting generated the granites now exposed in the High Himalaya (Debon *et al.* 1986; Scaillet *et al.* 1995; Le Fort *et al.* 1987). A pronounced satellite magnetic low is observed on the Tibetan Plateau and Alsdorf & Nelson (1999) showed that this could be modelled by a shallow Curie depth (16–18 km) across the entire Tibetan Plateau. Geothermal phenomena and high heat flow are also consistent with partial melting at depths of 20 km (Francheteau *et al.* 1984; Hochstein & Regenauer-Lieb 1998). Finally, several geodynamic models show that crustal melting is an inevitable consequence of crustal thickening (Henry *et al.* 1997; Beaumont *et al.* 2001).

What weaknesses are there in the hypothesis that partial melt is present beneath Southern Tibet? While a broad zone of relatively low melt fraction is consistent with the available data, the zones of very high melt fraction needed to explain the large reflection coefficients may be problematic. Complete crustal melting requires a temperature in excess of 900 °C (Murase & McBirney 1973) and it is not clear whether this occurs at a depth of 20 km in Southern Tibet (Chen & Molnar 1983; Henry *et al.* 1997; Ross *et al.* 2001). Could an alternative fluid be responsible for the low resistivity and large reflection coefficient? The seismic studies of the bright-spots suggest that saline fluids may provide a better fit to the amplitude-versus-offset data (Makovsky & Klemperer 1999).

5.4 Saline aqueous fluids

5.4.1 Conductivity of saline fluids

Saline aqueous fluids are good electrical conductors. Laboratory studies show that the electrical conductivity of an NaCl solution is dependent on the salinity, pressure and temperature (Sourirajan & Kennedy 1962). At low temperature (below 300 °C) the conductivity of an NaCl solution is relatively independent of pressure, while at higher temperatures the conductivity decreases with pressure (Quist & Marshall 1968). The critical point for a liquid is defined as the pressure–temperature conditions at which gases and liquids can coexist. Given that wet rocks begin to melt at 650 °C, this temperature

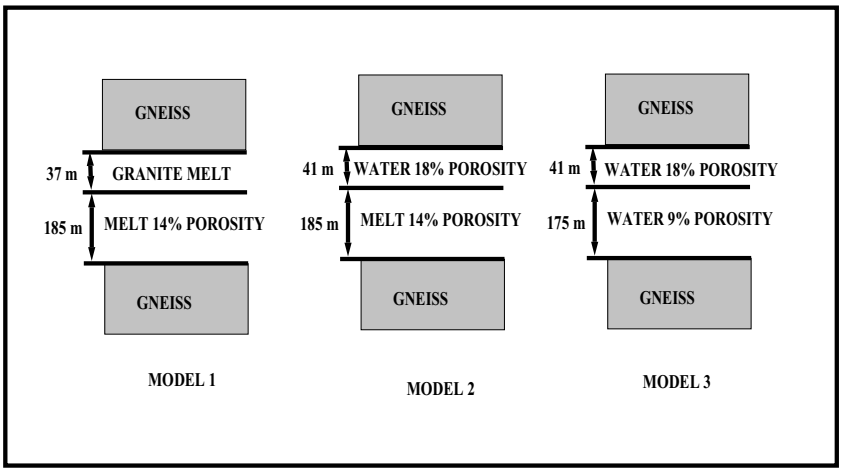

Figure 14. Possible models for Damxung bright spots (after Ross *et al.* 2001). Model 1, all melt; model 2, mixed model; model 3, all-water model. The most conductive model among these three is model 3.

can be considered the highest critical temperature for geothermal fluids. The critical pressure and salinity for this temperature are approximately 110 MPa and ∼25 per cent by weight (Olhoeft 1981). The NaCl concentration of crustal fluids varies from 0 to 40 per cent by weight (Jones 1992). Generally, the conductivity increases with salinity, but at very high concentrations of NaCl (>30 wt per cent) the conductivity of the solution decreases, ultimately becoming equal to the conductivity of molten NaCl (Nesbitt 1993).

To determine whether saline fluids could explain the high conductivity observed in Tibet, the composition of the fluid is required. Regrettably, this value is unknown. Thus we can only determine the minimum fluid content, by considering the maximum possible fluid conductivity. The highest salinity reported is approximately 25 per cent NaCl by weight, which corresponds to a maximum conductivity of around 100 S m^{-1} (Sourirajan & Kennedy 1962; Quist & Marshall 1968; Nesbitt 1993).

5.4.2 Interconnection of saline fluids

What degree of interconnectivity should we expect for aqueous fluids? Studies of fluid connectivity (Mibe *et al.* 1998; Minarik & Watson 1995) show that aqueous fluids can form an interconnected network at fluid fractions below <5 per cent. In a system containing a mixture of rock and fluid, the dihedral angle controls the interconnectivity of crustal fluids. It is the angle between the surface of the liquid and the rock and is controlled by surface energy. The fluids are confined to isolated pockets when this angle is greater than 60°, and interconnected when the angle is less than 60°. Laboratory studies of quartz saturated with aqueous fluids showed that increasing salinity could lower the dihedral angle to 40° (Watson & Brennan 1987). Since a significant salt content is required to produce a high conductivity, a dihedral angle lower than 60° and interconnection is expected for conditions in Southern Tibet. Petrologic studies of the dihedral angle (Holness 1998) confirm that aqueous fluids will be interconnected over a wide range of pressure and temperature conditions in middle and lower crustal rocks. Thus the Hashin–Shtrikman upper bound can be used to estimate the bulk conductivity of a rock containing aqueous fluids.

5.4.3 Model and agreement with other geophysical data

Using the upper bound of 100 S m^{-1} for the conductivity of a saline fluid, the fluid fraction–thickness combinations consistent with a conductance of 6000 S are shown in Fig. 13. Note that with a higher-conductivity fluid, a thinner layer is required to explain the observed conductance (i.e. a lower porosity or reduced thickness). For example, with 10 per cent porosity, a layer only 0.9 km can produce a conductance of 6000 S. With a fluid conductivity of 30 S m^{-1}, the layer needs to be 3 km thick (Fig. 13).

A thin, high-porosity, layer of aqueous fluids is broadly consistent with the characteristics of the seismic bright-spots. In addition, Makovsky & Klemperer (1999) suggest that the amplitude-versus-offset data are best explained with a thin layer of free aqueous fluids, although this is questioned by Ross *et al.* (2001). If the bright-spots are a result of free aqueous fluids, rather than a layer of melt, then this predicts lower crustal temperatures in Southern Tibet at depths of 15–20 km. This is consistent with the observations of earthquakes to depths of 15 km in this area (Chen & Molnar 1983). If this depth corresponds to the brittle–ductile transition, a temperature of 350 °C can be inferred. It is likely that an aqueous layer would have a porosity that varies with depth. Ross *et al.* (2001) show a model of this type (Fig. 14, model 3) that gave a good match to the observed seismic amplitudes and waveforms. Assuming that the aqueous fluid has a conductivity of 100 S m^{-1}, then model 3 has a total conductance of only ∼2000 S. With a lower fluid conductivity of 30 S m^{-1}, the conductance is only ∼500 S. Additional conductance is again needed to satisfy the MT data. This could be either a zone of lower porosity aqueous fluids or partial melt below the high-porosity layers in model 3.

However, there are a number of problems with the aqueous fluid hypothesis. A thin layer of free aqueous fluids cannot explain the INDEPTH passive seismic data (Kind *et al.* 1996), which detected an ∼20 km thick low-velocity zone. As in the discussion of partial melting, it must be stressed that MT data cannot distinguish thick and thin layers of the same conductance. This effectively means that the MT data cannot determine the porosity of the layer. What other information can be used to determine a range of realistic porosities for mid-crustal conditions? In the debate regarding the high conductivity of the continental lower crust, both graphite films and saline fluids have been suggested. Petrological studies have shown that there are problems maintaining an interconnected network of saline fluids at lower crustal conditions over significant timescales, and would suggest that the maximum fluid content would be around 0.1 per cent (Yardley 1986; Yardley & Valley 1997, 2000). At higher porosities waves of fluid motion would allow the fluid to escape rapidly (Connolly & Thompson 1989). Can the MT data be explained with a porosity of 0.1 per cent? Using the maximum conductivity of 100 S m^{-1}, this would require a layer 89 km thick. This is clearly unlikely since it would extend through the entire crust and into the upper mantle. If these arguments are applicable to stable continental interiors, then residence times are likely to be shorter in the dynamic environment of a tectonically active region such as Tibet. In summary, the presence of a layer of high-porosity, free aqueous fluids is inconsistent with the passive seismic data and some petrological observations.

5.5 Partial melt and aqueous fluids

The high-conductivity layer imaged by the MT data could be a result of a layer of partial melt or aqueous fluids. However, both of these explanations are inconsistent with various aspects of the geophysical and geological data in Southern Tibet. Is a model with a combination of partial melt and aqueous fluids the optimal solution? Seismic data give some support for this interpretation. Makovsky & Klemperer (1999) showed that the bright-spots have amplitude-versus-offset characteristics consistent with an aqueous layer. However, the waveform study of Ross *et al.* (2001) showed that a thin layer of water over partial melt (Fig. 14, Model 2) can also produce the measured reflection amplitudes. Model 3 has a maximum conductance of ∼2000 S and model 2 has a maximum conductance of 1450 S, much less than the minimum conductance of 6000 S derived in this study. Thus, an additional 4000 S of conductance is required to satisfy the MT data. The MT data are consistent with either partial melt or aqueous fluids below the thin layer in model 2 and 3.

What is the origin of the aqueous fluids in this combined aqueous fluid–melt model? They could be derived from the cooling of the deeper partially molten system. When wet crustal melts from the deep crust rise up to a depth where the temperature approaches the solidus, they crystallize. Then a phase rich in free water can separate from the saturated melt and collect above the cooling melt layer through buoyancy effects (Jahns 1982).

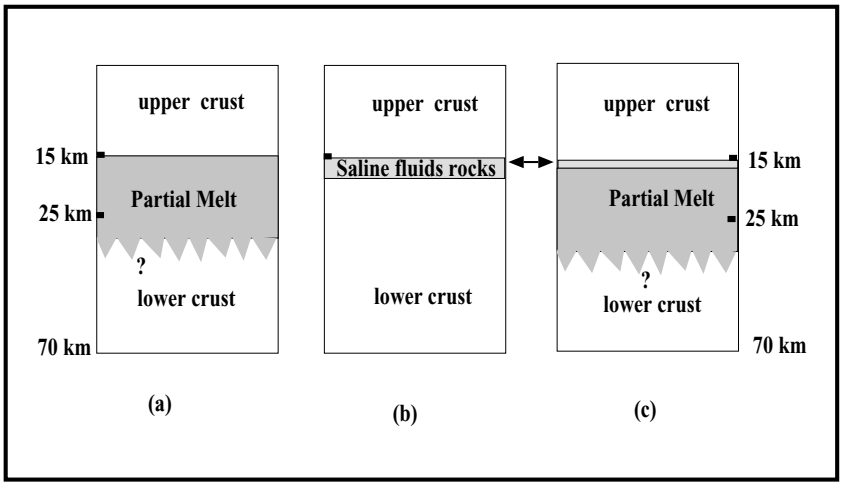

Figure 15. Three schematic models for high-conductivity crust in Southern Tibet. All models have normal upper and lower crust and a fluid fraction of 10–15 per cent in the conductive layer. The marked depth is not exact. Model (a) is characterized by a layer more than 10 km thick of partial melt. Model (b) contains an ∼1 km thick layer of 10–15 per cent saline fluids. Model (c) combines an ∼200 m thick layer of 10–15 per cent saline fluids above a thick (>10 km) layer of partial melt.

6 CONCLUSIONS AND TECTONIC IMPLICATIONS

The MT data presented in this study have shown that the conductance beneath the Lhasa Block is at least 6000 S. To account for this unusually high conductance, we have examined five possible explanations. The models invoking fluids appear to be the most likely, yet the MT and other available data cannot exclude any of the three models in Fig. 15 as possibilities. If the 6000 S conductance was solely caused by aqueous fluids, a range of thicknesses and porosity are possible. For example, a layer of 10 per cent porosity with a thickness 0.9–3.0 km (with 30 and 100 S m^{-1} fluids, respectively). Aqueous fluids alone are the least likely explanation, owing to its inconsistency with a thick low-velocity zone (Kind *et al.* 1996), and petrological arguments that question whether more than 0.1 per cent porosity is possible in mid and lower crustal conditions (Yardley & Valley 1997).

Owing to independent evidence for partial melting (Francheteau *et al.* 1984; Nelson *et al.* 1996; Alsdorf & Nelson 1999) and seismic reflection data (Ross *et al.* 2001), the melt and melt plus aqueous fluids are more likely explanations. There is some evidence that amplitude-versus-offset characteristics of the data may favour the uppermost fluid layer being free aqueous fluids (Makovsky & Klemperer 1999). The MT and reflection data may be best explained with a layer of 10–15 per cent aqueous fluid a few hundred metres thick overlying a thick (>10 km) layer of partial melt. As repeatedly stated in the paper, the MT data can only estimate the conductance of the fluid layer. Thus a continuum of aqueous fluid and melt models would also fit the data, with varying proportions of aqueous fluid and melt. In this context it should also be noted that the thickness shown in Fig. 15 does not imply that these values are required by the MT data. They are not required and are simply used to illustrate the approximate quantity of fluid required in each model.

The conductive layer shows significant lateral variations in conductance. This could be caused by changes in: (1) the porosity within the layer; (2) the layer thickness; (3) the degree of interconnection; or (4) the conductivity of the fluid. Changes arising from (4) are less likely than (1)–(3) since fluid composition depends on the subsurface geology, rather than pressure or temperature. Thus, lateral changes in the conductance have the potential to determine where more fluid is present, or alternatively where the fluid is most effectively connected.

High crustal conductances, with large spatial extents, are often found in active orogens and have been reported in the Andes (20 000 S, Echternacht *et al.* 1997; Brasse *et al.* 2002) and the Pyrenees (30 000 S, Pous *et al.* 1995). These authors attribute the high conductance to partial melting. High conductances are also found in extensional environments. Wannamaker *et al.* (1997) report a uniform conductor beneath the Eastern Great Basin that was attributed to a layer of aqueous fluids overlying a partial melt layer.

The widespread distribution of fluids is important since fluids can dramatically alter the rheology of a rock. When the melt fraction is close to the critical melt fraction (20–55 per cent), the rock loses significant strength (Renner *et al.* 2000). The presence of partial melt at much lower melt fractions also has mechanical effects, and is typified by enhanced creep rates and slow deformation (Cooper & Kohlstedt 1986). Aqueous fluids can also weaken a rock and enhance creep rates through a range of mechanisms (Etheridge *et al.* 1984; Tullis *et al.* 1996). A weakened layer in the mid or lower crust is required in geodynamic models that account for lithospheric deformation through crustal flow (Royden *et al.* 1997; Clark & Royden 2000). Thus, observations of a pervasive layer of crustal fluids in Southern Tibet show, in principle at least, that large-scale crustal flow could be occurring beneath Southern Tibet. The lower crustal flow can then accommodate the on-going east–west extension on the plateau and maintain a flat but highly dynamic plateau. The lateral variations in crustal conductance described above might also be significant in this context. If regions of high conductance are as a result of the highest fluid content or best fluid connection, then they might also represent the zones of most active crustal deformation, since they will be the weakest owing to the enhanced fluid content.

ACKNOWLEDGMENTS

Financial support of this work was provided by NSF grant EAR-9418822, EAR-9614590 and Geological Survey of Canada contribution no 2002133. The manuscript benefited from reviews by Bruce Yardley and Graham Heinson and editorial comments by Karsten Bahr. Field help from the MT group at the China University of

Geosicences (Wuhan) is gratefully acknowledged. Special thanks go to Barry Narod, Nong Wu, Ian Billings and Jiande Hu for their hard work during the field campaign.

REFERENCES

Allegre, C.J. *et al.*, 1984. Structure and evolution of Himalaya–Tibet orogenic belt, *Nature,* **307,** 17–22.

Alsdorf, D. & Nelson, K.D., 1999. Tibetan satellite magnetic low: evidence for widespread melt in the Tibetan crust?, *Geology,* **27,** 943–946.

Archie, G.E., 1942. The electrical resistivity log as an aid in determining some reservoir characteristics, *Trans. Am. Inst. Min. Metall. Pet. Eng.,* **146,** 54–62.

Argand, E., 1924. La tectonique de l'Asie, *Proc. 13th Int. Geol. Congr.,* pp. 170–372.

Armijo, R., Tapponnier, P., Mercier, J.L. & Han, T.L., 1986. Quaternary extension in Southern Tibet; field observations and tectonic implications, *J. geophys. Res.,* **91,** 13 803–13 872.

Beaumont, C., Jamieson, R.A., Nguyen, M.H. & Lee, B., 2001. Himalayan tectonics explained by extrusion of a low-viscosity crustal channel coupled to focused surface denudation, *Nature,* **414,** 738–742.

Brasse, H., Lazaeta, P., Rath, V., Schwalenburg, K., Soyer, W. & Haak, V., 2002. The Bolivian Altiplano Conductivity Anomaly, *J. geophys. Res.* **107 (B5),**10.1029/2001JB000391.

Brown, L.D. *et al.*, 1996. Bright spots, structure, and magmatism in Southern Tibet from INDEPTH seismic reflection profiling, *Science,* **274,** 1688–1690.

Camfield, P.A. & Gough, D.I., 1977. A possible proterozoic plate boundary in North America, *Can. J. Earth Sci.,* **14,** 1229–1238.

Chen, W. & Molnar, P., 1983. Focal depths of intracontinental and intraplate earthquakes and their implications for the thermal and mechanical properties of the lithosphere, *J. geophys. Res.,* **88,** 4183–4214.

Chen, L., Booker, J.R., Jones, A.G., Wu, N., Unsworth, M.J., Wei, W. & Tan, H., 1996. Electrically conductive crust in Southern Tibet from INDEPTH magnetotelluric surveying, *Science,* **274,** 1694–1696.

Clark, M.K. & Royden, L., 2000. Topographic ooze: building the eastern margin of Tibet by lower crustal flow, *Geology,* **28,** 703–706.

Cogan, M.J., Nelson, K.D., Kidd, W.S.F., Wu, C. & Project INDEPTH Team, 1998. Shallow structure of Yadong–Gulu rift, Southern Tibet, from refraction analysis of Project INDEPTH common midpoint data, *Tectonics,* **17,** 46–61.

Connolly, J.A.D. & Thompson, A.B., 1989. Fluid and enthalpy production during regional metamorphism, *Contrib. Mineral. Petrol.,* **102,** 347–366.

Cooper, R.F. & Kohlstedt, D.L., 1986. Rheology and structure of Olivine–Basalt partial melts, *J. geophys. Res.,* **89,** 9315–9323.

Copeland, P., Harrison, T.M., Yun, P., Kidd, W., Roden, M. & Yuquan, Z., 1995. Thermal evolution of the Gangdese batholith, Southern Tibet: a history of episodic unroofing, *Tectonics,* **14,** 223–236.

Coward, M.P., Kidd, W.S.F., Yun, P., Shackleton, R.M., Hu, Z., 1988. The structure of 1985 Tibet Geotraverse, Lhasa to Golmud, *Phil. Trans. R. Soc. Lond.,* A., **327,** 307–336.

Debon, F., Le Fort, P., Sheppard, S.M.F. & Sonet, J., 1986. The four plutonic belts of the Trans-Himalaya–Himalaya; a chemical, mineralogical, isotopic, and chronological synthesis along a Tibet–Nepal section, *J. Petrol.,* **27,** 219–250.

Dewey, J.F. & Burke, K.C., 1973. Tibetan, Variscan and Pre-Cambrian basement reactivation products of continential collision, *J. Geol.,* **81,** 683–692.

Echternacht, F., Tauber, S. Eisel, M., Brasse, H., Schwarz, G. & Haak, V., 1997. Electromagnetic study of the active continental margin in northern Chile, *Phys. Earth planet. Inter.,* **102,** 69–87.

Etheridge, M.A., Wall, V.J. & Cox, S.F., 1984. High fluid pressure during regional metamorphism and deformation: implications for mass transport and deformation mechanisms, *J. geophys. Res.,* **89,** 4344–4358.

Fielding, E., Isacks, B., Barazangi, M. & Duncan, C., 1994. How flat is Tibet?, *Geology,* **22,** 163–167.

Francheteau, J., Jaupart, C., Shen, X.J., Kang, W.H., Lee, D.L., Bai, J.C., Wei, H.P. & Deng, H.Y., 1984. High heat flow in Southern Tibet, *Nature,* **307,** 32–36.

Frost, B.R., Fyfe, W.S., Tazaki, K. & Chan, T., 1989. Grain-boundary graphite in rocks and implications for high electrical conductivity in the lower crust, *Nature,* **340,** 134–136.

Gamble, T.D., Goubau, W.M. & Clarke, J., 1979. Magnetotellurics with a remote reference, *Geophysics,* **44,** 53–68.

Guillot, S., Le Fort, P., Pecher, A., Barman, M.R. & Aprahamian, J., 1995. Contact metamorphism and depth of emplacement of the Manaslu granite (central Nepal). Implication for Himalayan orogenesis, *Tectonophysics,* **241,** 99–119.

Harrison, T.M., Copeland, P., Kidd, W.S.F. & Lovera, O.M., 1995. Activation of the Nyainquentanghla Shear Zone: implications for the uplift of the southern Tibetan Plateau, *Tectonics,* **14,** 658–676.

Hashin, Z. & Shtrikman, S., 1962. A variational approach to the theory of effective magnetic permeability of multiphase materials, *J. appl. Phys.,* **33,** 3125–3131.

Henry, P., Le Pichon, X. & Goffe, B., 1997. Kinematic, thermal and petrological model of the Himalayas: constraints related to metamorphism within the underthrust Indian crust and topographic elevation, *Tectonophysics,* **273,** 31–56.

Hochstein, M.P. & Regenauer-Lieb, K., 1998. Heat generation associated with collision of two plates the Himalayan geothermal belt, *J. Volc. Geotherm. Res.,* **83,** 75–92.

Holness, M.B., 1998. Contrasting rock permeability in the aureole of the Ballchulish igneous complex, Scottish Highlands: the influence of surface energy, *Contrib. Mineral. Petrol.,* **131,** 68–94.

Jahns, R.H., 1982. Internal evolution of pegmatite bodies, in *Short Course in Granitic Pegmatites in Science and Industry,* pp. 293–327, ed. Cerny, P., Mineralogical Association of Canada, Winnipeg.

Jones, A.G., 1992. Electrical conductivity of the continental lower crust, in *Continental Lower Crust,* pp. 81–143, eds Fountain, D.M., Arculus, R. & Key, R.W., Elsevier, Amsterdam.

Kind, R. *et al.*, 1996. Evidence from earthquake data for a partially molten crustal layer in Southern Tibet, *Science,* **274,** 1692–1694.

Lebedev, E.B. & Khitarov, N.I., 1964. Dependence on the beginning of melting of granite and the electrical conductivity of its melt on high water vapor pressure, *Geochem. Int.,* **1,** 193–197.

Le Fort, P., Cuney, M., Deniel, C., France-lanord, C., Sheppard, S.M.F., Upreti, B.N. & Vidal, P., 1987. Crustal generation of the Himalayan leucogranites, *Tectonophysics,* **134,** 39–57.

Macdonald, J.D., 1987. *Impedence Spectroscopy: Emphasizing Solid Materials and Systems,* Wiley, New York.

Makovsky, Y. & Klemperer, S.L., 1999. Measuring the seismic properties of Tibetan bright spots: free aqueous fluid in the Tibetan middle crust, *J. geophys. Res.,* **104,** 10 795–10 825.

Makovsky, Y., Klemperer, S.L., Ratschbacher, L., Brown, L.D., Li, M., Zhao, W. & Meng, F., 1996. INDEPTH Wide-angle reflection observation of *P*-wave-to- *S*-wave conversion from crustal bright spots in Tibet, *Science,* **274,** 1690–1691.

Maxwell, J.C., 1881. *A Treatise on Electricity and Magnetism,* 2nd edn, Clarendon, Oxford.

Mibe, K., Fujii, T. & Yasuda, A., 1998. Connectivity of aqueous fluid in the Earth's upper mantle, *Geophys. Res. Lett.,* **25,** 1233–1236.

Minarik, W.G. & Watson, E.B., 1995. Interconnectivity of carbonate melt at low melt fraction, *Earth planet. Sci. Lett.,* **133,** 423–437.

Murase, T. & McBirney, A.R., 1973. Properties of some common igneous rocks and their melts at high temperature, *Geol. Soc. Am. Bull.,* **84,** 3563–3592.

Navin, D.A., Peirce, C. & Sinha, M.C., 1998. The RAMESSES experiment; II, evidence for accumulated melt beneath a slow spreading ridge from wide-angle refraction and multichannel reflection seismic profiles, *Geophys. J. Int.,* **135,** 746–772.

Nelson, K.D. *et al.*, 1996. Partially molten middle crust beneath Southern Tibet: synthesis of project INDEPTH results, *Science,* **274,** 1684–1688.

Nelson, K.D. & the Project INDEPTH Team, 1999. Melt in the Tibetan Crust: where are we now?, *AGU Fall Meeting 1999,* Vol. 80, no 46, F991–F992, 1999/supplement.

Nesbitt, B., 1993. Electrical resistivity of crustal fluids, *J. geophys. Res.,* **98,** 4301–4310.

Nover, G., Heikamp, S., Meurer, H.J. & Freund, D., 1998. *In-situ* electrocal conductivity and permeability of mid-crustal rocks from the KTB drilling: consequences for high conductive layers in the Earth crust, *Surv. Geophys.,* **19,** 73–85.

Olhoeft, G., 1981. Electrical properties of granite with implications for the lower crust, *J. geophys. Res.,* **86,** 931–936.

Owens, T.J. & Zandt, G., 1997. Implications of crustal property variations for models of Tibetan plateau evolution, *Nature,* **387,** 37–43.

Pan, Y. & Kidd, W.S.F., 1992. Nyainqentangula shear zone: a late Miocene extensional detachment in the southern Tibetan Plateau, *Geology,* **20,** 775–778.

Parker, R.L., 1980. The inverse problem of electromagnetic induction: existence and construction of solution based upon incomplete data, *J. geophys. Res.,* **85,** 4421–4428.

Pous, J., Munoz, J.A., Ledo, J.J. & Liesa, M., 1995. Partial melting of subducted continental lower crust in the Pyrenees, *J. geol. Soc. Lond.,* **152,** 217–220.

Quist, A.S. & Marshall, W.L., 1968. Electrical conductances of aqueous sodium chloride solution from 0 to 800 °C at pressure to 4000 bars, *J. Phys. Chem.,* **72,** 684–703.

Renner, J., Evans, B. & Hirth, G., 2000. On the rheologically critical melt fraction, *Earth planet. Sci. Lett.,* **181,** 585–594.

Roberts, J.J. & Tyburczy, J.A., 1999. Partial-melt electrical conductivity: influence of melt composition, *J. geophys. Res.,* **104,** 7055–7065.

Ross, A.R., Brown, L.D., Alsdorf, D. & Nelson, K.D., 2002. Deep seismic bright spots and magmatism in Southern Tibet, *J. geophys. Res.,* in review.

Royden, L.H., Burchfiel, B.C., King, R.W., Wang, E., Chen, Z., Shen, F. & Liu, Y., 1997. Surface deformation and lower crustal flow in eastern Tibet, *Science,* **276,** 788–790.

Scaillet, B., Pecher, A., Rochette, P. & Champenois, M., 1995. The Gangotri Granite (Garhwal Himalaya); laccolithic emplacement in an extending collisional belt, *J. geophys. Res.,* **100,** 585–607.

Schmeling, H., 1986. Numerical models on the influence of partial melt on elastic, anelastic and electrical properties of rocks. Part II: electrical conductivity, *Phys. Earth planet. Inter.,* **43,** 123–136.

Sengor, A.M.C., 1981. The evolution of palaeo-tethys in the Tibetan segment of the Alpides, *Geological and Ecological studies of the Qinghai–Xizang Plateau,* Vol. 1, pp. 51–56, Science, Beijing.

Smith, J.T., 1995. Understanding telluric distortion matrices, *Geophys. J. Int.,* **122,** 219–226.

Smith, J.T. & Booker, J.R., 1991. Rapid inversion of two- and three-dimensional magnetotelluric data, *J. geophys. Res.,* **96,** 3905–3922.

Sourirajan, S. & Kennedy, G.C., 1962. The system H_2O-NaCl at elevated temperature and pressures, *Am. J. Sci.,* **260,** 115–141.

Tapponnier, P., Peltzer, G., Le Dain, A., Armijo, R. & Cobbold, P., 1982. Propagating extrusion tectonics of Asia, new insights from simple experiments with plasticine, *Geology,* **10,** 611–616.

Tullis, J., Yund, R. & Farver, J., 1996. Deformation-enhanced fluid distribution in feldspar aggregates and implications for ductile shear zones, *Geology,* **24,** 63–66.

Tyburczy, J.A. & Waff, H.S., 1983. Electrical conductivity of molten basalt and andesite to 25 kbar pressure: geophysical significance and implications for charge transport and melt structure, *J. geophys. Res.,* **88,** 2413–2430.

Ucok, H., 1979. Temperature dependence of the electrical resistivity of aqueous salt solutions and solution-saturated porous rocks, *PhD thesis*, University of Southern California, Los Angeles.

van Ngoc, P., Boyer, P., Therme, P., Yuan, X.C., LI, L. & Yin, G.Y., 1986. Partial melting zones in the crust of Southern Tibet from magnetotelluric results, *Nature,* **319,** 310–314.

Waff, H.S. & Weill, D.F., 1975. Electrical conductivity of magmatic liquids: effects of temperature, oxygen fugacity and composition, *Earth planet. Sci. Lett.,* **28,** 254–260.

Wannamaker, P.E., Johnston, J.M., Stodt, J.A. & Booker, J.R., 1997. Anatomy of the southern, Cordilleran hingeline, Utah and Nevada, from deep electrical resisitivity profiling, *Geophysics,* **62,** 1069–1086.

Watanabe, T., 1993. Effect of water an melt on seismic velocities and their application to characterization of seismic reflectors, *Geophys. Res. Lett.,* **20,** 2933–2936.

Watson, E.B. & Brennan, J.M., 1987. Fluids in the lithosphere, 1. Experimentally-determined wetting characteristics of CO_2–H_2O fluids and their implications for fluids transport, host-rock physical properties and fluids inclusion formation, *Earth planet. Sci. Lett.,* **85,** 497–515.

Wei, W. *et al.*, 2001. Detection of widespread fluids in the Tibetan Crust by magnetotelluric studies, *Science,* **292,** 716–718.

Willett, S.D. & Beaumont, C., 1994. Subduction of Asian lithospheric mantle beneath Tibet inferred from models of continental collision, *Nature,* **369,** 642–645.

Yardley, B.W.D., 1986. Is there water in the deep continental crust?, *Nature,* **323,** 111.

Yardley, B.W.D. & Valley, J.W., 1997. The petrologic case for a dry lower crust, *J. geophys. Res.,* **102,** 12 173–12 185.

Yardley, B.W.D. & Valley, J.W., 2000. Reply, *J. geophys. Res.,* **105,** 6065–6068.

Yin, A. & Harrison, T., 2000. Geological evolution of the Himalayan–Tibetan orogen, *Annu. Rev. Earth Planet. Sci.,* **28,** 211–280.

Zandt, G. & Ammon, C.J., 1995. Continental crust composition constrained by measurement of crustal Poisson's ratio, *Nature,* **374,** 152–154.

Zhao, W.L. & Morgan, W.J.P., 1987. Injection of Indian crust into Tibetan lower crust; a two-dimensional finite element model study, *Tectonics,* **6,** 489–504.